A Near-Field Cloaking Study to Reduce MRI RF-Artefacts in Presence of Elongated Prostheses

(Article begins on next page)

18 May 2024

A Near Field Cloaking Study to Reduce MRI RF-Artefacts in Presence of Elongated Prostheses

Umberto Zanovello, Luca Zilberti, and Ladislau Matekovits

Abstract—Objective: To analyze a near-field electromagnetic cloaking to reduce the radiofrequency (RF) magnetic field inhomogeneities (responsible for the RF-artefacts onset) in Magnetic Resonance Imaging (MRI) in presence of elongated metallic hardware.
Technology or Method: A lumped circuit is considered to explain the role that a dielectric coat has on hiding a metallic cylinder to the RF antenna. The theoretical assumptions are proved by means of full-wave simulations that are also applied to a realistic hip prosthesis.
Results: The numerical results confirm the theoretical assumptions. Both the theoretical analysis and the numerical simulations highlight the opposite role that the coat thickness and electric permittivity have in the definition of a proper dielectric coat.
Clinical or Biological Impact: A particular cloaking approach leads to a dielectric coat whose constitutive electrical parameters may be simple enough to fit the considered application reducing the interaction between an elongated prosthesis and the RF antenna.

Keywords—Magnetic Resonance Imaging, RF-Artefacts, electromagnetic cloaking, hip prosthesis.

I. INTRODUCTION

THE incidence of the total hip or total knee arthroplasty definitely increased in the last years [1], [2]. Hence, the importance of a proper investigation tool to recognize the presence of perioperative and/or postoperative diseases becomes evident. Thanks to high tissues contrast, spatial resolution, sensitivity and/or specificity, Magnetic Resonance Imaging (MRI) emerged over others clinical techniques in the evaluation of several pathologies resulting from a total joint arthroplasty [3]. In particular MRI emerges as the most sensitive method to quantify the location and extent of osteolysis and as the optimal mean to image nerves surrounding hip arthroplasty [4].

Metallic objects have been recognised to be one of the most important sources of artefacts in MRI. This kind of artefacts is originated by the interaction with the different types of electromagnetic fields generated inside the MRI scanner. Specific strategies are already in practice to face the artefacts produced by the interaction among the implants and the stationary or switched-gradient magnetic fields [5]–[13]. On the contrary, artefacts arising from the scattering produced by such objects in the RF field (B_1) still represent an open issue. In addition, taking into account the trend towards stronger static magnetic fields [14], an increment of the importance of the RF-induced artefacts has been registered in clinical platforms because of the corresponding increment in the RF field frequency [9], [11], [13]. Some solutions have been proposed in order to mitigate the RF-induced artefacts [12], [15]. Recently, the authors proposed to cover the prosthesis

with an Epsilon Near Zero (ENZ) ideal dielectric coat to hide it to the RF antenna [16]. In particular, they showed heuristically, by means of numerical simulations, that a 1 mm thick dielectric coat made with a zero-conductivity and 0.1 relative permittivity material, strongly decreases the RF-artefacts onset.

There is a substantial difference between most of the cloaking approaches proposed in literature [17]–[27] and this specific MRI application. In a far-field application, the disturbing object does not strongly interact with the source but it represents an obstacle to the field propagation. In this application, the object (i.e. the prosthesis) interacts with the source and it will be shown how it is possible to act on the object-antenna couplings to obtain an electromagnetic near-field cloaking.

Since the type of coupling depends also on the geometry of the involved components, it will be shown how it is possible to operate only on the prevailing kind of coupling to obtain relatively simple material parameters.

footnotetext In [16], the cloaking results were provided considering a specific coat whose properties were obtained through a heuristic procedure. In this work, a particular approach for near-field cloaking is presented by means of a simplified but effective circuital model and numerical simulations. On the basis of the obtained results, the relation between coat thickness and relative permittivity is investigated, identifying a systematic and flexible coat design procedure. Finally, it is shown how the effectiveness of the coat keeps almost the same if the relative permittivity is stressed only in a particular direction. The last simplification may be a key point in a possible future realization of the material.

U. Zanovello is a Ph.D. student in Electrical, Electronic and Telecomunications engineering at Politecnico di Torino (I-10129 Torino, Italy). He develops his activity in cooperation with the Istituto Nazionale di Ricerca Metrologica (I-10135 Torino, Italy) (e-mail: umberto.zanovello@polito.it).

L. Zilberti is with the Istituto Nazionale di Ricerca Metrologica (I-10135 Torino, Italy) (e-mail: l.zilberti@inrim.it)

L. Matekovits is with the Department of Electronics and Telecommunications, Politecnico di Torino (I-10129 Torino, Italy) and with the Macquarie University (NSW 2109 Sydney, Australia) (e-mail: ladislau.matekovits@polito.it)

"This paper is an expanded paper from the 2nd IEEE Conference on Advances in Magnetics, held from February 4 to February 7, 2018, at La Thuille, Italy.

II. METHODS

In the set-up depicted in Fig. 1(a), a generic 8-leg Birdcage coil surrounds a cylindrical phantom whose electrical properties are similar to those of some human tissues. A cylindrical metallic object (mimicking an elongated prosthesis) is plunged in the centre of the phantom. The Birdcage coil can generate a circularly polarized, highly homogenous, radiofrequency magnetic field B_1 [28]. Under ideal operating conditions, the currents flowing in two opposite legs of the Birdcage have
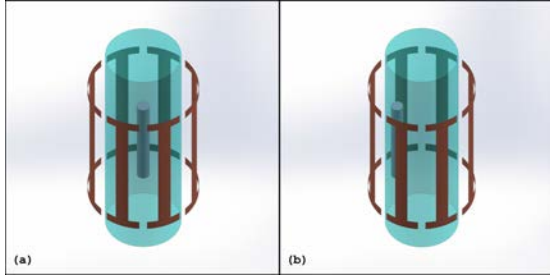
Fig. 1: A cylindrical phantom is placed inside an 8-leg Birdcage coil. A cylindrical metallic object is plunged into the phantom in a central (a) or lateral (b) position.
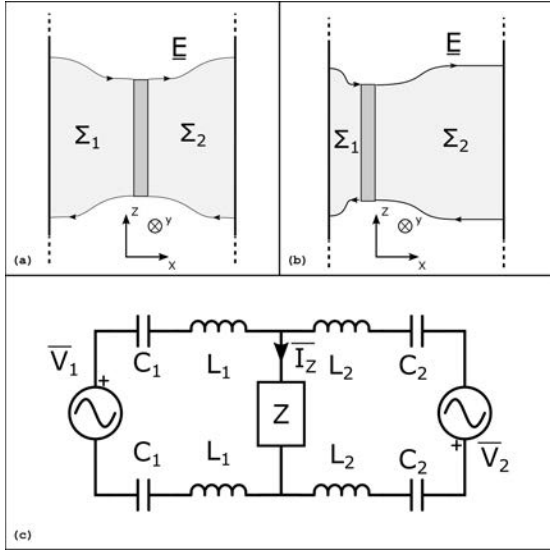

Fig. 2: Capacitive coupling between the loop coil and the central (a) or lateral (b) cylinder. The coupling between the loop coil and the tips of the cylinder is not represented. In (c), a simplified AC circuital model of the problem is reported.

opposite phase angles and the system is analogous to four planar coils where each coil is rotated by an angle $2\pi/8$ from the previous one. Due to the linearity of the problem, it is possible to consider each of the four planar loop coils separately and superpose their effects. The couplings between a loop coil and a generic external object can be, in principle, both inductive and capacitive [12], [29]–[31]. The firsts are due to the time-varying magnetic field that induces currents inside the object. In the case of an object with an electrical conductivity much higher than that of the background (i.e. the case of a metallic object in the considered phantom), such currents are almost bounded within the object itself. As regards the capacitive couplings, dielectric currents flow through the material surrounding the object, going from the source to the object itself. Dealing with elongated metallic objects, the inductive currents have a limited space to flow. It is hence reasonable to suppose that the effects on the B_1 homogeneity due to an inductive coupling may be, in first place, negligible if compared to the capacitive ones [29]. Fig. 2(a) qualitatively represents the capacitive coupling between the cylinder placed in the centre of the phantom (whose presence is neglected, in this simplified

analysis) and the loop coil lying on the xz-plane, whose height along the z-axis is much higher than that of the cylinder. Capacitive couplings occur with both sides of the loop and the peripheral electric field lines identify two surfaces Σ_1 and Σ_2. Fig. 2(c) reports an AC equivalent circuit that describes the problem. Z represents the cylinder impedance, whereas the capacitive couplings are accounted for by the capacitances C_1 and C_2 for the left and right side, respectively. L_1 and L_2 represent the inductive reactions. The induced voltages are obtained by the fluxes of the magnetic field through the Σ surfaces. Their signs are opposite in Fig. 2(c) because they both generate a clockwise current for a magnetic field oriented along the direction opposite to the y-axis. $\bar{I}_z$ represents the current due to the presence of the metallic cylinder and it is responsible for RF-artefacts. Due to the geometrical symmetry of the considered case, the induced voltages, capacitances and inductances (on the two sides of the load Z) have the same values. With these parameters, the solution of the circuit in Fig. 2(c) gives a zero current $\bar{I}_z$. The capacitances C_1 and C_2 may easily account for the presence of the phantom considering them as the series of the capacitance between the loop coil and the phantom and between the phantom and the metallic cylinder. However, the presence of the phantom does not affect the results because, due to symmetry, C_1 remains equal to C_2. This confirms the results obtained from simulations that do not show the rise of any artefacts (i.e. magnetic field perturbations outside the metallic object) when the metallic object is placed in the Birdcage centre. To highlight that this result is typical for elongated metallic objects (where the effects of capacitive couplings predominate), the case of a metallic toroid, where the inductive coupling is significant, has been examined. Results, not reported for brevity, show the rise of artefacts also in the case where the object is placed in the Birdcage coil centre.

The situation drastically changes when the metallic cylinder is moved laterally (Fig. 1(b)). Fig. 2(b) qualitatively represents the situation (numerical simulations supports the qualitative behaviour reported in Fig. 2(b)). In this condition, the induced voltages, capacitances and inductances become unbalanced. This causes the current $\bar{I}_z$ to be no longer zero with the effect of artefacts creation. In the next section, some simulations are presented as a confirmation of the obtained result. To decrease the value of $\bar{I}_z$ it is possible to act on the capacitance values as hereafter proposed. It is well-known that the capacitance value of the series of different capacitances is smaller than the smallest capacitance in the series. Thus, adding in series to C_1 and C_2 a smaller capacitance, it would result in a decreased $\bar{I}_z$ and, consequently, in an improvement of the B_1 homogeneity. By covering the metallic object with the coat, the generic equivalent capacitance for the examined problem becomes:

$$C_{eq} = \left(\frac{1}{C_{Bc-Ph}} + \frac{1}{C_{Ph-Co}} + \frac{1}{C_{Co-Obj}} \right)^{-1} \quad (1)$$

where C_{Bc-Ph} is the capacitance between the Birdcage coil and the phantom, C_{Ph-Co} is the capacitance between the phantom and the dielectric coat and C_{Co-Obj} is the capacitance between the coat and the metallic object. Covering the metallic object with a 1 mm coat made of a material with 0.1 relative

permittivity, causes C_{Co-Obj} to be much smaller than the other two components of (1). This results in a strong reduction of the equivalent capacitance and, consequently, in an artefacts decrease. For the sake of comparison, if the same ENZ coat is used to cover a centrally-placed metallic toroid, the artefacts remain unaltered, demonstrating that the dielectric coat has no effects on the inductive couplings.

Inspection of (1) shows that, when C_{Co-Obj} is much smaller than the other capacitances, C_{eq} is mainly determined by C_{Co-Obj} itself and therefore its value, in a first approximation, is proportional to the coat permittivity and inversely proportional to its thickness. Starting from this consideration, several simulations have been carried out to assess the influence that the thickness of the coat and its relative permittivity have on the artefacts reduction. Since the electric field lines, responsible for the capacitive coupling, are normal to the metallic surfaces, the possibility of applying an anisotropic dielectric coat has been also considered. Note that all comments developed for a metallic cylinder keep valid for an elongated metallic prosthesis. To prove this, in the result section the simulations are extended to the case of a realistic metallic hip prosthesis model.

In all simulations, an 8-leg Birdcage coil with a $175\,\mathrm{mm}$ radius and $460\,\mathrm{mm}$ height is driven in quadrature operating mode (to generate a circularly polarized magnetic field) at $128\,\mathrm{MHz}$. The metallic objects (a cylinder with a $20\,\mathrm{mm}$ radius and $300\,\mathrm{mm}$ height or a realistic $220\,\mathrm{mm}$ height femoral stem of a hip prosthesis) are plunged in a cylindrical phantom and placed $80\,\mathrm{mm}$ from its centre. In order to decrease the simulation time, without bringing to significant loss of information, all metallic parts have been simulated as perfect electric conductors (PEC). The phantom (radius: $120\,\mathrm{mm}$, height: $730\,\mathrm{mm}$) has a relative permittivity of 61.5 and an electrical conductivity of $0.87\,\mathrm{S/m}$. Such values are close to those characterizing some of the human tissues [32] at the frequency of interest. The power outgoing from each port of the Birdcage coil is set to obtain, in absence of any object inside the phantom, a magnetic field of $2.5\,\mathrm{\mu T}$ in its centre. To evaluate the effect of the metallic objects, the homogeneity of the clockwise component (B_1^+) [33] is analysed. In the result section, the homogeneity of B_1^+ on a given slice is normalized with respect to the maximum B_1^+ value of the same slice:

$$B_1^+(P)\Big|_{dB_{MAX}} = \frac{B_1^+(P)}{max(B_1^+)|_{slice}} \qquad (2)$$

To compare the homogeneity in different situations, the standard deviation of this quantity is reported. The standard deviation is evaluated both considering the whole slice (σ_{WS}) and only a subregion (identified by the black rectangles in the figures) surrounding the object (σ_{RA}). The zone inside the metallic objects (when present) is excluded from the computation of the standard deviation.

The simulations have been carried out by means of the frequency-domain solver of COMSOL Multiphysics®. To validate the numerical results, the same set-up (i.e. the metallic cylinder, placed laterally inside the phantom and coated by a 0.1 relative permittivity $1\,\mathrm{mm}$ thick coat) has been simulated through the frequency-domain solver of CST-MWS® finding

an excellent agreement.

III. RESULTS

In order to have a term of comparison for the results proposed below, some general results are reported in Fig. 3 (see also [16]). Fig. 3(a) and (d) report the empty phantom set-up, for the $z = 0\,\mathrm{mm}$ axial plane and the $y = 0\,\mathrm{mm}$ coronal plane, respectively. In the latter case, the computation of σ_{WS} has been limited from $z = -200\,\mathrm{mm}$ to $z = 200\,\mathrm{mm}$, to remove from the analysis the B_1^+ inhomogeneities due to the finite length of the coil. The standard deviation of B_1^+ evaluated on the whole slice is approximately equal to $0.7\,\mathrm{\mu T}$ for both planes. This parameter increases by 60% for the axial plane (Fig. 3(b)) and by 100% for the coronal plane (Fig. 3(e)) when the metallic cylinder is placed laterally. The situation is analogous when the realistic hip prosthesis model is considered. In Fig. 3(b),(c),(e),(f), the so-called "ghost" (i.e. the blue zone where the B_1^+ intensity is much lower than elsewhere) is appreciable. This is caused by the magnetic field generated by the dielectric currents that circulate in the phantom explaining the fact that the ghost may not touch the metallic object. The amplitude, paths and relative phase of these currents determine the size and position of the ghost.

In Fig. 4, some simulations, obtained with different types of coats, are proposed considering the lateral cylinder. In Fig. 4(a), (d) the set-up already proposed in a previous paper [16] is reported. A $1\,\mathrm{mm}$ thick coat, with a relative permittivity equal to 0.1 decreases the standard deviation to a value comparable to that obtained in the ideal case (i.e. without any object inside the phantom). Fig. 4(b) and (e) show the analogous situation when the cylinder is covered by a 0.4 relative permittivity coat. Dealing with the axial plane (Fig. 4(b)) the standard deviation increases by 40% for the whole slice and by more than 80% for a reduced area enclosing the cylinder with respect to the previous case. The rise of the standard deviation is less evident considering the coronal plane (Fig. 4(e)). It increases by approximately 35% for the whole slice and by 50% within reduced area. Although the result gets worse with respect to that obtained with a 0.1 relative permittivity, it still represents an improvement if compared to the uncoated case (see Fig. 3(b) and (e)). In particular, the standard deviation decreases by almost 15% considering the axial slice and by almost 25% considering the coronal plane. Fig. 4(c) and (f) show an interesting, even if not practical, result. Using a coat with $10\,\mathrm{mm}$ thickness, a relative permittivity equal to 1 (i.e., that of vacuum) would bring to standard deviations comparable to those obtained for the ideal case and for the $1\,\mathrm{mm}$ thick, 0.1 relative permittivity coat. This result confirms that, in first place, the dielectric constant of the coat and its thickness play an opposite role. The standard deviations reported in Fig. 4(c),(f) also take into account the B_1^+ inhomogeneities inside the coat. The standard deviation, computed for the reduced area in the coronal slice, further decreases to $0.67\,\mathrm{\mu T}$.

Fig. 5 shows some results concerning the realistic hip prosthesis model placed in a lateral position. In Fig. 5(a),(d), the prosthesis is covered by a $1\,\mathrm{mm}$ thick coat with 0.1 relative permittivity (see also [16]). Similarly to the cylinder case, the
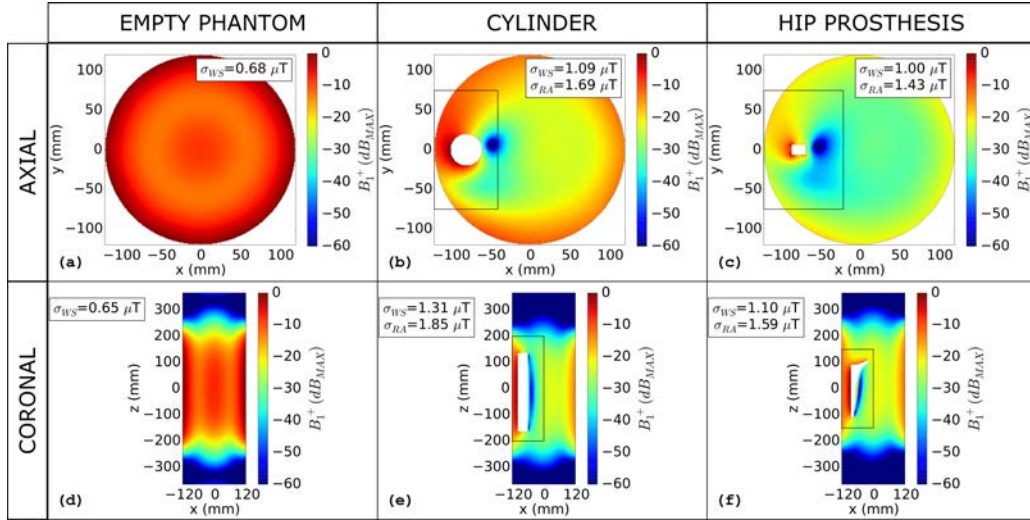
Fig. 3: B_1^+ (dB$_{MAX}$) evaluated for the ideal case without any object ((a) and (d)), with the metallic cylinder ((b) and (e)) and with the realistic hip prosthesis stem model ((c) and (f)) inside the phantom. The results are shown on the planes z = 0 ((a), (b) and (c)) and y = 0 ((d), (e) and (f)).
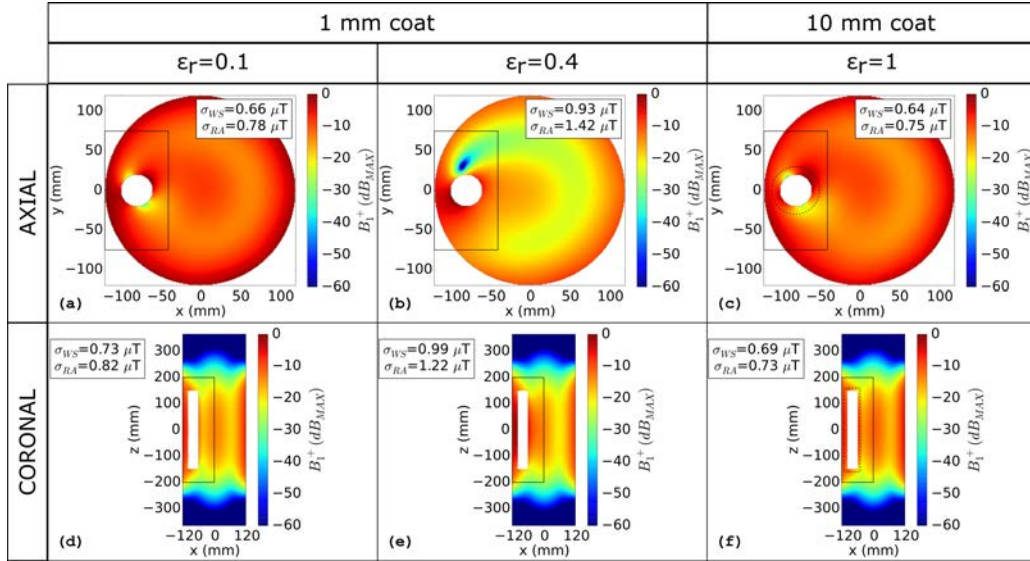

Fig. 4: B_1^+ (dB$_{MAX}$) evaluated with the cylinder placed laterally. Results are shown on the planes z = 0 ((a), (b) and (c)) and y = 0 ((d), (e) and (f)). In (a) and (d) the cylinder is covered with a 1 mm thick, 0.1 relative permittivity coat. In (b) and (e) the cylinder is covered with a 1 mm thick, 0.4 relative permittivity coat. Finally, in (c) and (f) the cylinder is covered with a 10 mm thick, 1 relative permittivity coat. The dashed lines in (c) and (f) represent the coat size.

standard deviations decrease, becoming comparable to those obtained for the unperturbed case. Fig. 5(b),(e) show the effect of a 3 mm thick coat with the relative permittivity of vacuum. Due to the prosthesis shape, it turns out that such a coat would bring to satisfying cloaking results with a still limited geometrical influence of the coat on the hip stem. As for the cylinder (Fig. 4(c),(f)), also Fig. 5(e),(f) seem to confirm the opposite roles that the dielectric permittivity of the coat and its thickness play in hiding the object. The slight differences in some standard deviations may be attributable to the fact that such a thickness inevitably results in varying the object shape. Finally, no sensible differences are appreciated if the coat is not considered in the computation of the standard deviation.

Fig. 6 reports the standard deviations evaluated in the axial plane for different simulated set-ups involving the cylindrical object. The standard deviations proposed in Fig. 6(a) have been computed on the whole xy slice, whereas those of Fig. 6(b) have been computed within a reduced area embracing the cylinder. In the lower part of the panels, several thickness/permittivity combinations are considered. Both for the whole slice case (a) and for the reduced area (b), the standard deviation on the main diagonal remains almost constant. This confirms again the opposite role of the coat thickness and permittivity. Another interesting standard deviation behaviour is obtained when the relative permittivity is increased keeping the thickness constant. Focusing on the coat thickness equal to 1 mm, it can
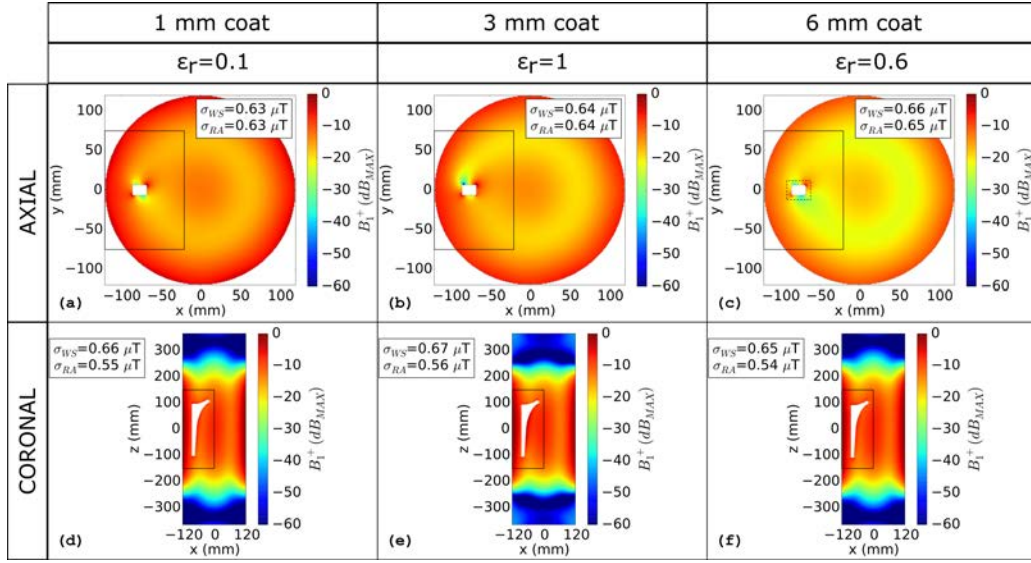
Fig. 5: B_1^+ (dB$_{MAX}$) evaluated with the prosthesis model placed laterally. Results are shown both on the axial ((a), (b) and (c)) and coronal ((d), (e) and (f)) planes. In (a) and (d) the prosthesis is covered with a 1 mm thick, 0.1 relative permittivity coat. In (b) and (e) the cylinder is covered with a 3 mm thick, 1 relative permittivity coat. Finally, in (c) and (f) the cylinder is covered with a 6 mm thick, 0.6 relative permittivity coat. The dashed lines in (c) and (f) represent the coat size.
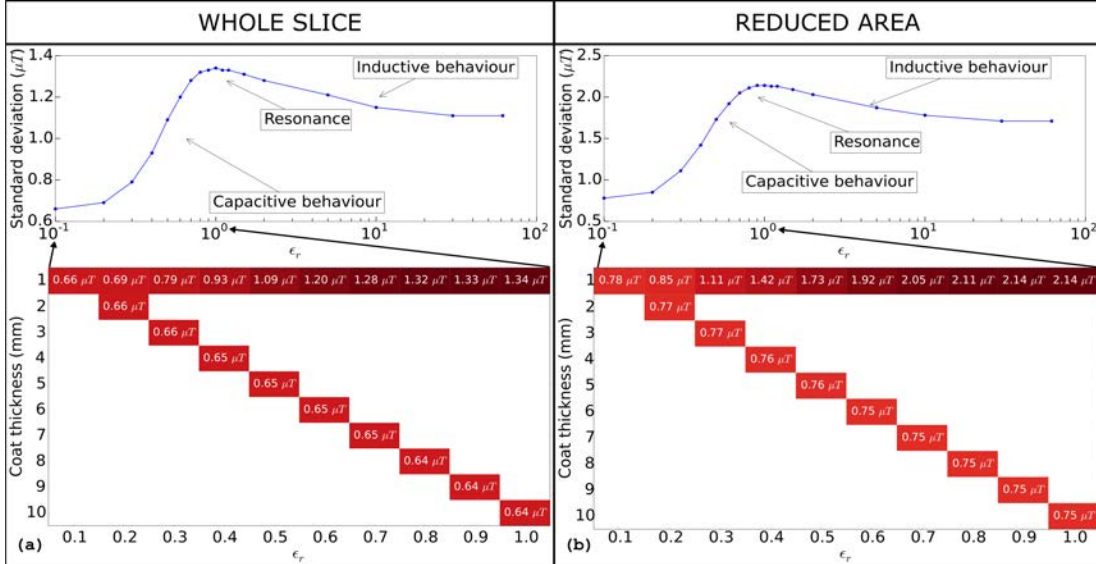

Fig. 6: Standard deviations evaluated for the metallic cylinder placed laterally inside the phantom. The axial z = 0 slice is considered both in (a) and in (b). The values of σ_{WS} are reported in (a) (see the map in the bottom) with different coat permittivity and thickness. The curve in the upper part refers to the 1 mm thickness. The same results are reported in (b) for a reduced area embracing the prosthesis.

be noticed that the standard deviation reaches values that are higher than those obtained without the coat. The uncoated case may be intended, in first place and for thin coat, as a coated case where the coat permittivity is equal to that of the phantom. It follows that a non-monotonic trend is obtained. This aspect is more appreciable in the curves reported in the upper parts of the panels of Fig. 6, where the permittivity is extended up to 61.5 (i.e., the phantom one). This behaviour can be explained by means of the equivalent circuit of Fig. 2(c), considering a generic series of a capacitance and an inductance

supplied by a generic AC voltage generator operating at a given frequency. For low values of relative permittivity, the capacitive reactance predominates over the inductive one. If a zero capacitance value (i.e. a zero permittivity) is considered, the series behaves as an open circuit. When the capacitive reactance approaches the inductive one, a resonance occurs. If the capacitance value increases further, the circuit becomes inductive. The behaviour of the equivalent circuit of Fig. 2(c) is comparable to that described above. Since the current in Z and the standard deviation are correlated, this explains the trends
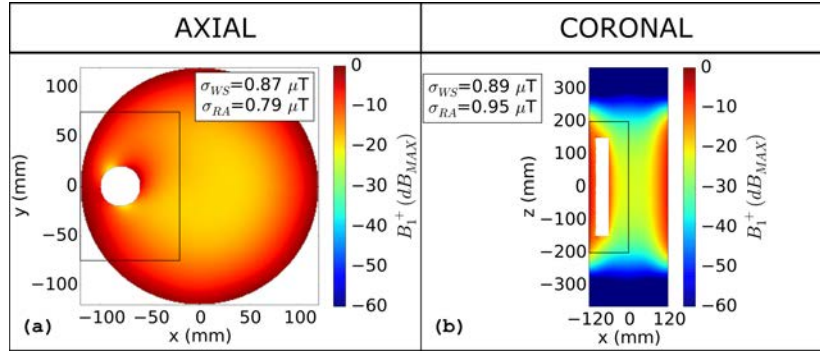
Fig. 7: B_1^+ (dB$_{MAX}$) evaluated with the cylinder placed laterally. Results are shown both on the axial plane z = 0 (a) and on the coronal plane y = 0 (b). The object is covered with a 1 mm thick, anisotropic coat. The coat presents a 0.1 relative permittivity along the direction normal to the cylinder surface and a relative permittivity equal to 2.5 along the other directions.

of the curves in Fig. 6. Note that a resistive term should be added to the equivalent circuit in order to obtain the dumped behaviour of the curves. This term is given, in the simulations, by the non-zero conductivity of the phantom and it is not modelled in the equivalent circuit of Fig. 2(c).

Finally, Fig. 7 shows the B_1^+ (dB$_{MAX}$) chromatic maps when the cylinder is covered with a 1 mm thick anisotropic coat. The permittivity tensor is settled to be 0.1 along the direction normal to the cylinder faces and 2.5 (a reasonable permittivity value for some common dielectric materials) along the other directions. Even if the permittivity along the directions not normal to the cylinder surface is twenty-five fold higher, the cloaking results are satisfying. In particular, the standard deviations computed in the reduced areas embracing the object decrease by approximately 50% for both planes with respect to the uncoated cylinder case. Furthermore, the B_1^+ ghost reported by the uncoated cases (see Fig. 3(b),(c),(e),(f)), that would inevitably result in a black spot in the diagnostic image, does not appear. Note that the origin of the differences with respect to the isotropic coat may be found in the behaviour of the electric field near the coat edges. In these zones, due to the particular coat geometry and permittivity tensor definition, the direction along which the relative permittivity is equal to 0.1 does not coincide with that of the electric field.

IV. Discussion

The results confirm the physical theory proposed in the Method section for a metallic cylinder. Nevertheless, some results are proposed also for a realistic hip prosthesis stem showing that all findings remain valid.

In this work, the benefits of the coat are shown in terms of the "transmit sensitivity" (B_1^+). Due to the symmetry of the problem, the same advantages would be appreciable with the receiver sensitivity (B_1^-) [33] resulting in the reduction of the signal losses in reception.

The core of the proposed method is based on a lumped elements circuital interpretation of an electromagnetic phenomenon. Of course, the proposed circuital model is a first approximation and does not take into account all possible phenomena that occur in the specific problem. For example, a resistor should be added in parallel to the "phantom-coat" capacitance to model

the phantom conductivity. For these reasons, the proposed circuit is not suitable to obtain quantitative results. The aim of the equivalent circuit is to give a qualitative and simple description of the basic principles on which a near-field cloaking application may be based. Due to the particular constitutive parameters required by the coat, a material that fits the considered application should be, in principle, synthesized as metamaterial (or meta-composite). Even if a material with a relative permittivity equal to that of vacuum has been shown to be effective for some configurations, a zero-conductivity material with suitable mechanical properties may not be so easily achievable. The study of metamaterials in MRI is a topic that has been investigated in the last years [34]–[39] even though, as far as the authors know, they have never been applied for a cloaking application. Indeed, the narrowband nature of metamaterials perfectly fits the MRI application where the frequency of the B_1 field is univocally determined and limited in a range of a few tens of kilohertz. The application proposed in this work presents several design constraints. Firstly, the coated prosthesis should present mechanical characteristics comparable to those of the uncoated one. Furthermore, the coat materials should be made totally biocompatible and not subjected to degradation. As for the relative permittivity, it may be "relaxed" increasing the coat thickness. However, the thickness of the coat does not have to influence the original shape and dimensions of the prosthesis. Being the metamaterials constitutionally anisotropic, the satisfying results shown by the anisotropic coat may be providential in a potential practical realization.

V. Conclusion

This study investigates the physical interpretation of the role of a dielectric coat applied to reduce RF-artefacts due to the presence of elongated metallic hardware in MRI. The results represent a key point for the design and realization of a suitable material. Furthermore, the paper introduces and demonstrates a particular near-field cloaking approach to face a well-known problem in MRI. Future work will deal with the research of a metamaterial configuration or meta-composite whose properties fit those of the specific application.

References

[1] H. Kremers *et al.*, "Prevalence of total hip and knee replacement in the united states," *Journal of Bone and Joint Surgery - American Volume*, vol. 97, no. 17, pp. 1386–1397, 2014. DOI: 10.2106/JBJS.N.01141.

[2] "13th annual report," National Joint Registry, Tech. Rep., 2016. [Online]. Available: http://www.njrcentre.org.uk/njrcentre/Portals/0/Documents/England/Reports/13th%20Annual%20Report/07950%20NJR%20Annual%20Report%202016%20ONLINE%20REPORT.pdf.

[3] P. Aliabadi *et al.*, "Cemented total hip prosthesis: Radiographic and scintigraphic evaluation," *Radiology*, vol. 173, no. 1, pp. 203–206, 1989. DOI: 10.1148/radiology.173.1.2675184.

[4] H. G. Potter *et al.*, "What is the role of magnetic resonance imaging in the evaluation of total hip arthroplasty?" *HSS Journal*, vol. 1, no. 1, pp. 89–93, 2005, ISSN: 1556-3324. DOI: 10.1007/s11420-005-0112-4.

[5] B. Hargreaves *et al.*, "Metal-induced artifacts in mri," *American Journal of Roentgenology*, vol. 197, no. 3, pp. 547–555, 2011. DOI: 10.2214/AJR.11.7364.

[6] S.-E. Song *et al.*, "Biopsy needle artifact localization in mri-guided robotic transrectal prostate intervention," *IEEE Transactions on Biomedical Engineering*, vol. 59, no. 7, pp. 1902–1911, 2012. DOI: 10.1109/TBME.2012.2192118.

[7] J. Schenck, "The role of magnetic susceptibility in magnetic resonance imaging: Mri magnetic compatibility of the first and second kinds," *Medical Physics*, vol. 23, no. 6, pp. 815–850, 1996. DOI: 10.1118/1.597854. [Online]. Available: https://www.scopus.com/inward/record.uri?eid=2-s2.0-0030013529&doi=10.1118%2f1.597854&partnerID=40&md5=085ab9e313cb55d087eea1634a8300a5.

[8] K. Koch *et al.*, "Magnetic resonance imaging near metal implants.," *Journal of magnetic resonance imaging : JMRI*, vol. 32, no. 4, pp. 773–787, 2010. DOI: 10.1002/jmri.22313. [Online]. Available: https://www.scopus.com/inward/record.uri?eid=2-s2.0-79952196693&doi=10.1002%2fjmri.22313&partnerID=40&md5=ee9141a0e62cf690ca47cab294e9b74a.

[9] H. Graf *et al.*, "Metal artifacts caused by gradient switching," *Magnetic Resonance in Medicine*, vol. 54, no. 1, pp. 231–234, 2005. DOI: 10.1002/mrm.20524.

[10] A. Shenhav and H. Azhari, "Gradient field switching as a source for artifacts in mr imaging of metallic stents," *Magnetic Resonance in Medicine*, vol. 52, no. 6, pp. 1465–1468, 2004. DOI: 10.1002/mrm.20294.

[11] H. Graf *et al.*, "Rf artifacts caused by metallic implants or instruments which get more prominent at 3 t: An in vitro study," *Magnetic Resonance Imaging*, vol. 23, no. 3, pp. 493–499, 2005. DOI: 10.1016/j.mri.2004.12.009.

[12] C. Camacho *et al.*, "Nonsusceptibility artifacts due to metallic objects in mr imaging," *Journal of Magnetic Resonance Imaging*, vol. 5, no. 1, pp. 75–88, 1995. DOI: 10.1002/jmri.1880050115.

[13] U. Lauer *et al.*, "Radio frequency versus susceptibility effects of small conductive implants - a systematic mri study on aneurysm clips at 1.5 and 3 t," *Magnetic Resonance Imaging*, vol. 23, no. 4, pp. 563–569, 2005. DOI: 10.1016/j.mri.2005.02.012. [Online]. Available: https://www.scopus.com/inward/record.uri?eid=2-s2.0-20344395132&doi=10.1016%2fj.mri.2005.02.012&partnerID=40&md5=f2981ad261b980434c4defef2f20e11f.

[14] F. Schick, "Whole-body mri at high field: Technical limits and clinical potential," *European Radiology*, vol. 15, no. 5, pp. 946–959, 2005. DOI: 10.1007/s00330-005-2678-0. [Online]. Available: https://www.scopus.com/inward/record.uri?eid=2-s2.0-22844444193&doi=10.1007%2fs00330-005-2678-0&partnerID=40&md5=f62d1cdacd024d197c8ae989f68bc7ad.

[15] T. Bachschmidt *et al.*, "Polarized multichannel transmit mri to reduce shading near metal implants," *Magnetic Resonance in Medicine*, vol. 75, no. 1, pp. 217–226, 2016. DOI: 10.1002/mrm.25621.

[16] U. Zanovello *et al.*, "An ideal dielectric coat to avoid prosthesis rf-artefacts in magnetic resonance imaging," *Scientific Reports*, vol. 7, no. 1, 2017. DOI: 10.1038/s41598-017-00215-7.

[17] A. Ward and J. Pendry, "Refraction and geometry in maxwell's equations," *Journal of Modern Optics*, vol. 43, no. 4, pp. 773–793, 1996. DOI: 10.1080/09500349608232782.

[18] J. Pendry *et al.*, "Controlling electromagnetic fields," *Science*, vol. 312, no. 5781, pp. 1780–1782, 2006. DOI: 10.1126/science.1125907.

[19] J. Prat-Camps *et al.*, "A magnetic wormhole," *Scientific Reports*, vol. 5, 2015. DOI: 10.1038/srep12488.

[20] C. Lan *et al.*, "Electrostatic field invisibility cloak," *Scientific Reports*, vol. 5, 2015. DOI: 10.1038/srep16416.

[21] B. Wood and J. Pendry, "Metamaterials at zero frequency," *Journal of Physics Condensed Matter*, vol. 19, no. 7, 2007. DOI: 10.1088/0953-8984/19/7/076208.

[22] D. Shin *et al.*, "Broadband electromagnetic cloaking with smart metamaterials," *Nature Communications*, vol. 3, 2012. DOI: 10.1038/ncomms2219.

[23] Y. Ma *et al.*, "First experimental demonstration of an isotropic electromagnetic cloak with strict conformal mapping," *Scientific Reports*, vol. 3, 2013. DOI: 10.1038/srep02182.

[24] J. Zhu *et al.*, "Three-dimensional magnetic cloak working from d.c. to 250 khz," *Nature Communications*, vol. 6, 2015. DOI: 10.1038/ncomms9931.

[25] H. Ma and T. Cui, "Three-dimensional broadband ground-plane cloak made of metamaterials.," *Nature communications*, vol. 1, p. 21, 2010.

[26] L. Li *et al.*, "Reconfigurable all-dielectric metamaterial frequency selective surface based on high-permittivity ceramics," *Scientific Reports*, vol. 6, 2016. DOI: 10.1038/srep24178.

[27] X. Wang *et al.*, "Implementation of low scattering microwave cloaking by all-dielectric metamaterials," *IEEE Microwave and Wireless Components Letters*, vol.

23, no. 2, pp. 63–65, 2013. DOI: 10.1109/LMWC.2013. 2238914.

[28] J. Tropp, "The theory of the bird-cage resonator," *Journal of Magnetic Resonance (1969)*, vol. 82, no. 1, pp. 51–62, 1989. DOI: 10.1016/0022-2364(89)90164-9.

[29] V. Ballweg *et al.*, "Rf tissue-heating near metallic implants during magnetic resonance examinations: An approach in the ac limit," *Medical Physics*, vol. 38, no. 10, pp. 5522–5529, 2011. DOI: 10.1118/1.3637495.

[30] W. Nitz *et al.*, "On the heating of linear conductive structures as guide wires and catheters in interventional mri," *Journal of Magnetic Resonance Imaging*, vol. 13, no. 1, pp. 105–114, 2001. DOI: 10.1002/1522-2586(200101)13:1<105::AID-JMRI1016>3.0.CO;2-0.

[31] M. Negishi *et al.*, "Origin of the radio frequency pulse artifact in simultaneous eeg-fmri recording: Rectification at the carbon-metal interface," *IEEE Transactions on Biomedical Engineering*, vol. 54, no. 9, pp. 1725–1727, 2007. DOI: 10.1109/TBME.2007.891940.

[32] S. Gabriel *et al.*, "The dielectric properties of biological tissues: Ii. measurements in the frequency range 10 hz to 20 ghz," *Physics in Medicine and Biology*, vol. 41, no. 11, pp. 2251–2269, 1996. DOI: 10.1088/0031-9155/41/11/002.

[33] D. Hoult, "The principle of reciprocity in signal strength calculations - a mathematical guide," *Concepts in Magnetic Resonance*, vol. 12, no. 4, pp. 173–187, 2000. DOI: 10.1002/1099-0534(2000)12:4<173::AID-CMR1>3.0.CO;2-Q.

[34] I. Connell *et al.*, "Design of a parallel transmit head coil at 7t with magnetic wall distributed filters," *IEEE Transactions on Medical Imaging*, vol. 34, no. 4, pp. 836–845, 2015. DOI: 10.1109/TMI.2014.2370533.

[35] M. Freire *et al.*, "On the applications of mu(r) = - 1 metamaterial lenses for magnetic resonance imaging," *Journal of Magnetic Resonance*, vol. 203, no. 1, pp. 81–90, 2010. DOI: 10.1016/j.jmr.2009.12.005.

[36] M. Wiltshire *et al.*, "Microstructured magnetic materials for rf flux guides in magnetic resonance imaging," *Science*, vol. 291, no. 5505, pp. 849–851, 2001. DOI: 10.1126/science.291.5505.849.

[37] R. Syms *et al.*, "Magneto-inductive catheter receiver for magnetic resonance imaging," *IEEE Transactions on Biomedical Engineering*, vol. 60, no. 9, pp. 2421–2431, 2013. DOI: 10.1109/TBME.2013.2258020.

[38] O. Zhuromskyy *et al.*, "2d metamaterials with hexagonal structure: Spatial resonances and near field imaging," *Optics Express*, vol. 13, no. 23, pp. 9299–9309, 2005.

[39] R. Schmidt *et al.*, "Flexible and compact hybrid metasurfaces for enhanced ultra high field in vivo magnetic resonance imaging," *Scientific Reports*, vol. 7, no. 1, 2017.